JOURNAL OF AIRCRAFT
Vol. 32, No. 5, September–October 1995

Decomposition-Based Optimization Procedure for High-Speed Prop-Rotors Using Composite Tailoring

Aditi Chattopadhyay,* Thomas R. McCarthy,† and Charles E. Seeley†
Arizona State University, Tempe, Arizona 85287-6106

A multilevel optimization procedure is developed to investigate the effect of changes in blade planform and composite tailoring on blade aerodynamic and structural performance of prop-rotor aircraft. Both high-speed cruise and hover performance are considered simultaneously. A composite box beam model is used to represent the principal load carrying member in the rotor blade. The upper level objective is to simultaneously maximize the high-speed cruise propulsive efficiency and the hover figure of merit using planform design variables. Constraints are imposed on other aerodynamic performance requirements and also on the physical dimensions of the blade. The lower-level objective is to reduce the critical tip displacements in both hover and cruise using composite tailoring. Optimization is performed using a nonlinear programming approach in the upper level and integer programming technique in the lower level. Optimum designs are compared with the XV-15 rotor blade performance at 300 kn, which is used as a baseline or reference design, and also with the results obtained from a purely aerodynamic optimization procedure. The results show significant improvements in both the aerodynamic and structural performance.

Nomenclature

c = chord, ft
F = axial force, lb
g_j = constraint function vector
H = interpolation matrix
k_{ij} = stiffness matrix, psi
M_y = flapping moment, lb-in.
M_z = lagging moment, lb-in.
P = random number, $0 < P < 1$
P_{acc} = acceptance probability
$\bar{Q}_{ij}$ = off-axis stiffness matrix for each lamina, psi
Q_y = transverse horizontal shear force, lb
Q_z = transverse vertical shear force, lb
R = blade radius, ft
r = radial location, ft
r_c = simulated annealing cooling rate
T = thrust, lb
T_k = simulated annealing "temperature"
t = wall thickness, in.
t/c = thickness-to-chord ratio
u, v, w = elastic displacements
x, y, z = reference axes
α_{zl} = zero lift angle, deg
$\gamma^0_{x\eta}, \gamma^0_{x\zeta}$ = shear strains
ε = blade strain
η_{ax} = rotor propulsive efficiency
η, ζ = local blade element axes
θ = blade twist, deg
κ = box beam scaling factor
Λ = blade sweep, deg
λ = out of plane warping function
σ_1, σ_2 = material axis normal stresses, psi
τ_{12} = shear stress, psi
ϕ = elastic twist
Φ = design variable vector
Ω = rotor angular velocity, rpm

Received June 17, 1994; revision received Nov. 28, 1994; accepted for publication March 10, 1995.

*Assistant Professor, Department of Mechanical and Aerospace Engineering. Senior Member AIAA.
†Graduate Research Assistant, Department of Mechanical and Aerospace Engineering. Member AIAA.

Introduction

RECENTLY, there has been a revival of interest in Short Haul Civil Transport (SHCT) prop-rotor aircraft such as the XV-15 tiltrotor. The goal of this class of aircraft is to operate with fixed-wing type efficiencies in cruise while maintaining the desirable hovering capabilities of a helicopter. Associated with these design goals are several conflicting requirements.[1-3] For example, high helical tip Mach numbers M_{tip} are a critical performance issue in high-speed cruise (350–450 kn). There are several ways of addressing this issue. The tip Mach number can be reduced through rotor tip speed reduction or through the use of blade sweep that reduces the effective Mach number. An alternative is to increase the drag divergence Mach number M_{DD} at the tip to values above M_{tip}. This can be accomplished through reductions in the blade thickness. However, each of these options will adversely affect the hover performance, drive system weight, or aeroelastic stability of the rotor blade. In the helicopter mode, to maintain a high figure of merit in hover, the solidity of the blade must be increased since thinner airfoils are used for maintaining efficiency in cruise. Due to these conflicting requirements associated with the performance of the aircraft in hover, in conversion, and in airplane modes, the application of formal optimization procedure is well suited to investigate the design tradeoffs. Recently, research efforts have been initiated by Chattopadhyay et al.[4-9] to develop formal optimization techniques to address these issues. In Refs. 4 and 5 optimization procedures were developed to maximize the high-speed cruise propulsive efficiency without degrading the hover figure of merit. An optimization procedure was developed in Ref. 6 to address to the problem of aeroelastic stability of high-speed prop-rotors. In Ref. 7, the drive system weight was minimized and the associated tradeoffs in cruise efficiency were investigated. The integrated aerodynamic, aeroelastic, and structural optimization problem was addressed in Ref. 8. More recently, McCarthy et al.[9] developed a purely aerodynamic multiobjective optimization procedure for improved high-speed cruise and hovering performance using planform and airfoil characteristics as design variables.

The structural behavior of the high-speed prop-rotor is also an integral part of the overall rotor performance. It is there-

fore essential that an accurate structural model be implemented. Composite blades have become increasingly popular in recent years due to the high stiffness and reduced weight offered by these materials. The use of composites also allows tailoring capabilities that can be used to improve the rotor structural and dynamic behavior. In this article, the aerodynamic and structural design criteria in both high-speed cruise and in hover are addressed by developing a multilevel decomposition-based optimization procedure. At the upper level, the aerodynamic performance of prop-rotors is optimized for both high-speed cruise and hover using planform variables. Constraints are imposed on the rotor thrust in hover and in cruise. At the lower level, the rotor is optimized for improved structural performance using composite ply orientations as design variables. Since the lower level optimization involves discrete design variables, an optimization procedure, based on simulated annealing technique,[10] is developed to address this complex problem. The results of the optimization procedure are compared with an existing rotor.[11]

For the aerodynamics analysis, an algorithm based on blade element momentum approach[12] is used. The procedure offers a significant reduction in computational effort from more comprehensive procedures that were previously used by Chattopadhyay and McCarthy.[4-8] The use of this analysis within an optimization procedure also provides realistic design trends as demonstrated by McCarthy et al.[9] The structural analysis is performed using a composite box beam model that includes blade pretwist, taper, and sweep to represent the principal load-carrying member in the blade. In this research, a quasi-one-dimensional composite beam theory, based on the model developed by Smith and Chopra,[13] is extended to include beam pretwist, taper, and spanwise sweep. The procedure offers significant computational savings from more refined finite element models while maintaining sufficient accuracy.

Multilevel Optimization Problem

Multidisciplinary design optimization of rotary wing aircraft can be a computationally intensive task if all of the disciplines involved are coupled with the optimizer and the optimization is performed "all-at-once" in a single level. Decomposition techniques, through which such complex optimization problems can be reduced into a number of subproblems, can be very effective in addressing this issue. Recently, such techniques have been applied to rotary wing optimization problems.[14,15] In this article, the multilevel decomposition procedure is used to address the complex multidisciplinary issues associated with high-speed prop-rotor design. The optimization procedure is decomposed into two levels. At the upper level the aerodynamic performance is improved, and at the lower level the objective is to improve the structural performance of the blade using composite tailoring. The upper and lower levels are coupled through the use of optimal sensitivity parameters,[15] which are essential in maintaining proper coupling between the levels. The following is a description of the decomposition and the optimization problem formulation.

Upper Level

At this level, the axial efficiency in high-speed cruise η_{ax} and the hover figure of merit (FM) are maximized simultaneously. Constraints are imposed on the physical dimensions of the blade to ensure that the load-carrying member of the rotor is maintained within the dimensions of the airfoil. The blade is discretized and design variables include the values of the chord c, twist θ, thickness to chord ratio t/c, and zero lift angle of attack α_{zl} at each node. The sweep distribution, however, is not discretized in order to ensure continuity of the elastic axis. The lifting line is assumed to be a quadratic function of the following form:

$$y_{a/c} = d_1 x + d_2(4x^2 - 3x) \tag{1}$$

where $y_{a/c}$ is the position of the aerodynamic center measured from the leading edge of the chord. The aerodynamic center is assumed to coincide with the elastic axis of the load-carrying structural member used in the problem formulation. The coefficients that determine the position of the aerodynamic center, d_1 and d_2, are used as design variables. Note that the functions associated with these coefficients [$f_1(x) = x$ and $f_2(x) = 4x^2 - 3x$] are orthogonal to each other, which is a favorable characteristic for optimization. The sweep distribution can then be formulated using this expression as follows:

$$\begin{aligned}\Lambda(y) &= \tan^{-1}(dy/dx) \\ &= \tan^{-1}[d_1 + d_2(8x - 3)]\end{aligned} \tag{2}$$

The optimization problem is stated as follows:

$$\begin{aligned}&\text{Maximize} && \text{FM}(\boldsymbol{\Phi}),\ \eta_{ax}(\boldsymbol{\Phi}) \\ &\text{Subject to} && T_{\text{hover}} = (T_{\text{hover}})_{\text{ref}} \\ &&& T_{ax} = (T_{ax})_{\text{ref}} \\ &&& \kappa t_{\text{hor}} \le t_{\max}\end{aligned}$$

where $\boldsymbol{\Phi} = [c(y),\ \theta(y),\ \Lambda(y),\ \alpha_{zl}(y),\ t/c(y)]$ is the design variable vector and the subscript "ref" indicates reference rotor value. The quantity t_{hor} is the thickness of the horizontal wall in the box beam, $t_{\max}$ is the maximum thickness of the airfoil, and κ is a scaling factor used to ensure that the box beam is maintained within the airfoil cross section.

Since the optimization problem involves more than one design objective, the problem is formulated using the Kreisselmeier–Steinhauser (K–S) function approach.[16] Using this approach the multiple objective functions and constraints are transformed into a single envelope function that is then minimized. The problem thus reduces to an unconstrained optimization problem. The K–S function technique has been found to perform very well in multiobjective rotary wing optimization problems.[6-9,15]

Lower Level

The objective at this level is to minimize the tip displacements in hover and in cruise. The most critical displacements in hover are the vertical displacement w_h and the elastic twist ϕ_h. In cruise, the elastic twist ϕ_c and the inplane displacement v_c are important. Therefore, these four displacements are selected as the individual objective functions to be minimized. Ply orientations are used as design variables. However, to avoid impractical orientations, the ply angles are chosen from a set of standard values [0, ±15, ±30, . . . , 90 deg]. The Tsai–Wu failure criterion[17] is used, which assumes that to avoid material failure, the following equation representing a failure surface in stress-space must be satisfied:

$$\begin{aligned}&\left(\frac{1}{\sigma_{1T}} - \frac{1}{\sigma_{1C}}\right)\sigma_1 + \left(\frac{1}{\sigma_{2T}} - \frac{1}{\sigma_{2C}}\right)\sigma_2 + \frac{\sigma_1^2}{\sigma_{1T}\sigma_{1C}} \\ &\quad - \frac{\sigma_1\sigma_2}{\sqrt{\sigma_{1T}\sigma_{1C}\sigma_{2T}\sigma_{2C}}} + \frac{\sigma_2^2}{\sigma_{2T}\sigma_{2C}} + \frac{\tau_{12}^2}{\tau_{12}^2 s} < 0\end{aligned} \tag{3}$$

where σ_1 and σ_2 represent normal stresses along the material axes and τ_{12} represents the shear stress. The subscripts T, C, and s represent the ultimate stress in tension, compression, and shear, respectively (see Fig. 1). This reduces the total number of constraints as individual constraints on the stress (σ_1, σ_2, and τ_{12}) at each ply are avoided. Each of the composite plates used in the box beam modeling are assumed to be symmetric about the midplane of the plate and the beam itself is assumed to be symmetric about its local axes, η and ζ (Fig. 2). Therefore, the earlier failure criterion is imposed, on each

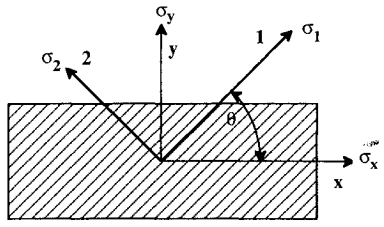

Fig. 1 Composite lamina material axes.

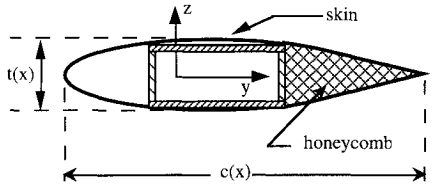

Fig. 2 Blade cross section.

lamina, at each of the four corners of the box beam to prevent failure due to stresses.

Analysis

Aerodynamic Analysis

The aerodynamic formulation is based on the model initially developed by Smith[18] and later modified by Talbot.[12] In this approach, the two-dimensional aspects of rotorcraft airfoils are modeled more accurately than the traditional two-dimensional airfoil theory. Compressibility and Reynolds number effects are included in this formulation. Further, analytical closed-form expressions are available for the calculation of aerodynamic performance in terms of variables such as planform, camber, and thickness. This allows for variations of these parameters during optimization for complete investigation of the effect of aerodynamic parameters on performance. The blade element theory used in the algorithm is due to Glauert.[19] An empirical fit was performed on NACA 63 and 64 series airfoil families in order to supply a functional relationship between maximum lift coefficient and the sectional thickness and camber for incompressible flow. The analysis is easily implemented within an optimization procedure and offers significant computational advantages from more comprehensive codes. The algorithm has been found to correlate extremely well with advanced technology blades and the procedure also yields meaningful design trends when used in a formal optimization procedure.[9] This code has been further modified by the authors to account for spanwise sweep to include sweep as a design variable. Further details of this analytical technique are found in Ref. 9. The aerodynamic analysis is coupled with a structural analysis that is described next. Therefore, the results of the complete analysis represent trimmed static solutions that include the effects of elastic deformations.

Structural Analysis

The load-carrying member of the rotor is modeled as a single-celled composite box beam (Fig. 2). In addition to the structural member inside the airfoil, the weights of the honeycomb structure and the blade skin are also included in the total weight calculation. The blade is discretized using finite elements with 19 total degrees of freedom U_e and unequal element sizes. Using the finite element model, it is possible to incorporate blade pretwist and sweep distributions into the problem formulation. The nodal degrees of freedom are described as follows:

$$U_e^T = (u_1, u_2, u_3, u_4, v_{b1}, v'_{b1}, v_{b2}, v'_{b2}, w_{b1}, w'_{b1}, w_{b2}, w'_{b2}, \phi_1, \phi_2, \phi_3, v_{s1}, v_{s2}, w_{s1}, w_{s2}) \quad (4)$$

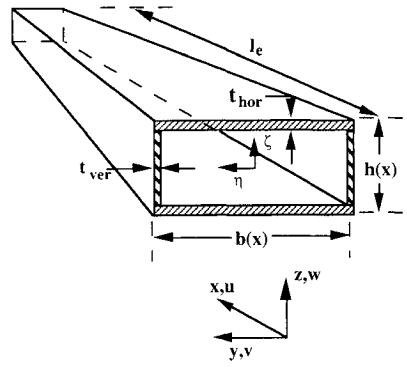

Fig. 3 Composite box beam.

where u is the axial displacement, v and w are the inplane horizontal and vertical displacements, and ϕ is the elastic twist. First partial derivatives with respect to the spanwise axis x are denoted ($'$). The formulation assumes that the inplane displacements can be decoupled into a term corresponding to pure bending and a term corresponding to shear as shown:

$$v = v_b + v_s \quad (5)$$

$$w = w_b + w_s \quad (6)$$

where the subscript b refers to the displacement due to beam bending and the subscript s refers to the displacements due to shear. Identical node locations are used in specifying both aerodynamic and structural parameters.

The outer dimensions of the box beam (Fig. 3) are constant percentages of the chord and thickness. Each composite plate used to model the composite box beam is assumed to be symmetric about the midplane of the plate. Each plate is made up of 24 laminated orthotropic composite plies. Further, the box beam is assumed to have double symmetry about the local coordinate axes (η and ζ). This ensures that the two vertical walls are identical to each other and also that the two horizontal walls are identical. The vertical and horizontal walls, however, are assumed to be independent of each other. The beam cross section is described by stretching, bending, twisting, shearing, and torsion-related warping. The stress–strain (σ–ε) relationships in the vertical and horizontal walls are written as follows:

$$\begin{Bmatrix} \sigma_{xx} \\ \sigma_{\zeta\zeta} \\ \sigma_{x\zeta} \end{Bmatrix}_v = \begin{bmatrix} \bar{Q}_{11} & \bar{Q}_{12} & \bar{Q}_{16} \\ \bar{Q}_{12} & \bar{Q}_{22} & \bar{Q}_{26} \\ \bar{Q}_{16} & \bar{Q}_{26} & \bar{Q}_{66} \end{bmatrix}_v \begin{Bmatrix} \varepsilon_{xx} \\ \varepsilon_{\zeta\zeta} \\ \varepsilon_{x\zeta} \end{Bmatrix}_v \quad (7)$$

$$\begin{Bmatrix} \sigma_{xx} \\ \sigma_{\eta\eta} \\ \sigma_{x\eta} \end{Bmatrix}_h = \begin{bmatrix} \bar{Q}_{11} & \bar{Q}_{12} & \bar{Q}_{16} \\ \bar{Q}_{12} & \bar{Q}_{22} & \bar{Q}_{26} \\ \bar{Q}_{16} & \bar{Q}_{26} & \bar{Q}_{66} \end{bmatrix}_h \begin{Bmatrix} \varepsilon_{xx} \\ \varepsilon_{\eta\eta} \\ \varepsilon_{x\eta} \end{Bmatrix}_h \quad (8)$$

where the subscripts v and h indicate vertical and horizontal walls, respectively. The off-axis stiffness matrix for each lamina is denoted $\bar{Q}_{ij}$ ($i, j = 1, 2$ and 6). The strains in the vertical walls are expressed as follows:

$$\varepsilon_{xx} = u' - \eta(v'' - \gamma^{0\prime}_{x\eta}) - \zeta(w'' - \gamma^{0\prime}_{x\zeta}) - \lambda\phi'' \quad (9)$$

$$\varepsilon_{x\zeta} = \left(\eta - \frac{\partial\lambda}{\partial\zeta}\right)\phi' + \gamma^0_{x\zeta} \quad (10)$$

$$\varepsilon_{\zeta\zeta} = a_0 u' + b_1\eta(v'' - \gamma^{0\prime}_{x\eta}) - c_2\zeta(w'' - \gamma^{0\prime}_{x\zeta}) - (d_0 + d_1\eta + d_2\zeta)\phi' + (f_0 + f_2\zeta)\gamma^{0\prime}_{x\eta} + (g_0 + g_1)\gamma^0_{x\zeta} \quad (11)$$

where u is the axial displacement, v and w are the horizontal and vertical inplane displacements, respectively, ϕ is the twist angle, and $\gamma^0_{x\eta}$ and $\gamma^0_{x\xi}$ represent the inplane shear stresses (Fig. 3). The superscript (′) represents second partial derivatives with respect to x. Similar expressions are obtained for the horizontal walls. The out-of-plane warping is denoted λ and the coefficients a_0–g_1 are determined such that the net inplane forces and moments in the horizontal and vertical walls are zero. Using these conditions, the equations of equilibrium are written as follows:

$$\begin{Bmatrix} F \\ Q_y \\ Q_z \end{Bmatrix} = \begin{bmatrix} k_{11} & k_{12} & k_{13} \\ k_{12} & k_{22} & 0 \\ k_{13} & 0 & k_{33} \end{bmatrix} \begin{Bmatrix} u' \\ \gamma^0_{x\eta} \\ \gamma^0_{x\xi} \end{Bmatrix} \tag{12}$$

$$\begin{Bmatrix} T \\ M_y \\ M_z \end{Bmatrix} = \begin{bmatrix} k_{44} & k_{45} & k_{46} \\ k_{45} & k_{55} & 0 \\ k_{46} & 0 & k_{66} \end{bmatrix} \begin{Bmatrix} \phi' \\ w'' - \gamma^{0\prime}_{x\xi} \\ v'' - \gamma^{0\prime}_{x\eta} \end{Bmatrix} \tag{13}$$

where M_z and M_y are the lagging and flapping moments, respectively, and T is the torsional moment. The axial force is denoted F, the inplane horizontal and vertical shear forces are denoted Q_y and Q_z, respectively, and k_{ij} $(i, j = 1, 2, \ldots, 6)$ represent the stiffness matrix elements. Further details of the formulation can be found in Ref. 13.

The elemental equilibrium equations are written in vector form as follows:

$$\boldsymbol{F}_e = \boldsymbol{K}_e \boldsymbol{u}_e \tag{14}$$

where $\boldsymbol{F}_e = (F\ Q_y\ Q_z\ T\ m_x\ m_z)^T$ is the elemental force vector, $K_e = [k_{ij}]$ is the elemental stiffness matrix, and $\boldsymbol{u}_e = [u'\ \gamma^0_{x\eta}\ \gamma^0_{x\xi}\ \phi'\ (v'' - \gamma^{0\prime}_{x\eta})\ (w'' - \gamma^{0\prime}_{x\xi})]^T$ represents the elemental degrees of freedom in the local coordinate system. Using these principles a finite element approach is developed using the weak formulation as follows:

$$\int_0^R \boldsymbol{H}_G \boldsymbol{F}_G \, dx = \int_0^R \boldsymbol{H}_G \boldsymbol{K}_G \boldsymbol{H}_G \boldsymbol{U}_G \, dx \tag{15}$$

where $\boldsymbol{F}_G$ and $\boldsymbol{K}_G$ are the global force vector and stiffness matrix, respectively, $\boldsymbol{U}_G$ is the global vector of discrete nodal degrees of freedom, and $\boldsymbol{H}_G$ is the global representation of the interpolation matrix. The blade displacements are written in the discretized element form as shown:

$$u(s) = \boldsymbol{H}(s)\boldsymbol{U}_e \tag{16}$$

where $\boldsymbol{H}(s)$ represents the complete set of interpolation vectors and the elemental nodal displacement vector.

Optimization Implementation

The multilevel optimization technique used in this research decomposes the design problem into a level where only continuous design variables are used (upper level) and a second level where discrete design variables are used (lower level). Therefore, two separate optimization strategies are necessary. Since traditional optimization techniques minimize only a single objective function, it is necessary to transform the original objective functions, at each level, using multiobjective function techniques. The technique used for each level is the K–S function approach,[16,20] which utilizes a composite envelope function to transform the original constrained and multiple objective function optimization problem into a single objective, unconstrained optimization problem. Further details of this technique are found in Refs. 5, 9, and 20. A nonlinear programming procedure (NLP) based on the Davidon–Fletcher–Powell algorithm (DFP) is used at the upper level. For the lower level, an optimization procedure has been developed based on the method of simulated annealing,[21] which is described next.

If ply angles are used as continuous design variables and are later rounded off to the nearest practical value (e.g., 17.3 deg being rounded off to 17 deg), the result can lead to suboptimal designs.[21] Allowing the ply angles to vary within a set of prescribed values during optimization is a more efficient approach. Therefore, in the structural optimization problem, the plies are selected from within a set of preselected orientations of integer multiples of ±15 deg, such as 0, ±15, ±30, . . . , 90 deg. This reduces the problem into a discrete optimization problem and conventional gradient-based optimization procedures are no longer applicable. Using the procedure developed in the current work, the optimization problem is transformed into a completely discrete problem. The new discrete problem can now be optimized using a simulated annealing technique that has been shown to be effective in a variety of different engineering applications.[22–24] The procedure developed is outlined next.

The multiobjective optimization problem is stated as follows:

$$\begin{aligned} &\text{Minimize } F_K(a_i) && K = 1, 2, \ldots \text{NF} \\ &\text{Subject to } g_M(a_i) && M = 1, 2, \ldots \text{NC} \\ & && i = 1, 2, \ldots \text{NDV} \end{aligned}$$

where NF is the number of objective functions, NC is the number of constraints, NDV is the number of design variables, and $\boldsymbol{a}$ is the vector of design variables. The ith design variable can assume any value from the design variables vector of preselected values, d_{iq} such as 0, ±15, ±30, . . . , 90 deg for ply angles. Therefore, the objective functions and constraints are completely represented by discrete design variables. The multiobjective optimization problem is transformed into a single unconstrained composite function to be minimized using the K–S function approach as previously described. An optimal solution cannot be guaranteed for a discrete optimization problem without evaluating every possible combination of discrete variables, which is computationally impractical. Near-optimal solutions can be obtained, however, with significant improvements in all objective functions with a reasonable amount of computational effort.

The simulated annealing algorithm is described briefly as follows:

START
Current design is F
Perturb current design F_{new}
If $F_{\text{new}} \le F$ then
  $F = F_{\text{new}}$
Else if $P_{\text{acc}} \ge P$ then
  $F = F_{\text{new}}$
End if
Go to START

where F is the objective function to be minimized and P is a random number such that $0 \le P \le 1$. The acceptance probability P_{acc} of retaining a worse design is computed as follows:

$$P_{\text{acc}} = \exp[(\Delta F/T_k)] \tag{17}$$

where ΔF is the change in the objective function and T_k is the "temperature" that is reduced during successive iterations, to ensure smooth convergence, according to

$$T_k = (r_c)^k T_0 \tag{18}$$

where T_0 is the initial temperature and r_c is the cooling rate that determines the temperature at the kth iteration. This reduces the probability of accepting a worse design. Occasionally accepting a worse design under the given probability allows the algorithm to climb out of possible local minima. The previous loop is repeated a prescribed number of times for each cycle in the multilevel optimization procedure.

Results

The reference rotor used is an existing advanced three-bladed gimballed rotor.[11] The aerodynamic optimization is performed at a cruise altitude of 25,000 ft and a forward velocity of 300 kn, with a rotational speed of 421 rpm. A vehicle weight of 13,000 lb and aircraft lift-to-drag ratio L/D of 8.4 is assumed. Therefore, the thrust in cruise is constrained to be 774 lb for the two-engine aircraft. In hover, the aircraft is assumed to be operating at sea level conditions with a rotational speed of 570 rpm and a 12% download effect from the rotor/wing interaction. The thrust in hover is therefore constrained to be 7280 lb. The blade is discretized into 10 segments (11 node points). The composite material used in the structural analysis is carbon-PEEK AS4/APC2.[25]

At the upper level the design variables for c, θ, α_{zl}, and t/c are all based on discrete nodal values, whereas the sweep distribution Λ is assumed to be based on a quadratic lifting line. This yields a total of 46 design variables. The scaling factor κ, used in the upper level constraints to ensure that the box beam is maintained in the airfoil, is assumed to vary as follows:

$$\kappa = \begin{cases} 4.0 & r < 0.8 \\ 3.0 & 0.8 \le r < 0.95 \\ 2.5 & 0.95 \le r \le 1.0 \end{cases} \tag{19}$$

where r is the nondimensional radial location. The reason for this variation is to ensure the validity of thin wall theory at inboard sections of the blade, since the majority of the load is carried in this section, without being too restrictive at the tip where thinner airfoils can improve the aerodynamic performance. The tolerance on the lower level objective functions, used as optimal sensitivity parameters at this level, is initially 5%. This value is reduced to 0.5% after six complete multilevel cycles in order to ensure that there is very little degradation of lower level objective functions at the upper level. The program KSOPT,[20] which is based on the DFP algorithm, is used for optimization at this level.

At the lower level, the discrete values of the ply orientations are used as design variables. Since a symmetric and balanced layup is used in both the vertical and horizontal walls, this leads to 12 independent design variables that can assume any of the seven preselected values of ply-angle orientations. The design space associated with this problem therefore consists of nearly 14 billion (7^{12}) possible combinations. The actual number of loops used at each multilevel cycle is 1000 iterations, which represents only a very small portion of the total design space. The value of the K–S function multiplier ρ used at this level is initially set to 5.0, but is subsequently reduced to 1.0 after four multilevel iterations. This is done to increase the sensitivity of the K–S function to changes in all of the objective functions and constraints. The cooling rate r_c used in the simulated annealing algorithm is 0.995 and the initial temperature T_0 is set to 1.0.

Convergence of the multilevel optimization procedure is achieved in seven cycles, where a cycle represents an individually converged optimization including both upper and lower levels. The initial design used in this optimization procedure corresponds to the optimal results obtained from a purely aerodynamic optimization using the same aerodynamic analysis.[9] The results from the multilevel-based optimization are compared to the design obtained from the purely aerodynamic optimization and also to a reference rotor that represents the original XV-15 prop-rotor. The results are presented in Table 1 and Figs. 4–12.

The upper level objective functions are presented in Fig. 4. It is shown in the figure that the hover FM, which is increased by 6.6% in the purely aerodynamic procedure, is further increased in the multilevel optimization (7.5%) compared to the reference rotor. The propulsive efficiency in high-speed cruise (η_{ax}) is increased by 3.6% from the reference rotor in the aerodynamic formulation and in the multilevel

Table 1 Ply orientation angles

	Optimum	
Reference, deg	Horizontal wall, deg	Vertical wall, deg
Outer ply		
0	15	0
0	−15	0
0	0	15
0	0	−15
15	15	30
−15	−15	−30
15	15	15
−15	−15	−15
45	30	45
−45	−30	−45
45	30	15
−45	−30	−15
Midplane		

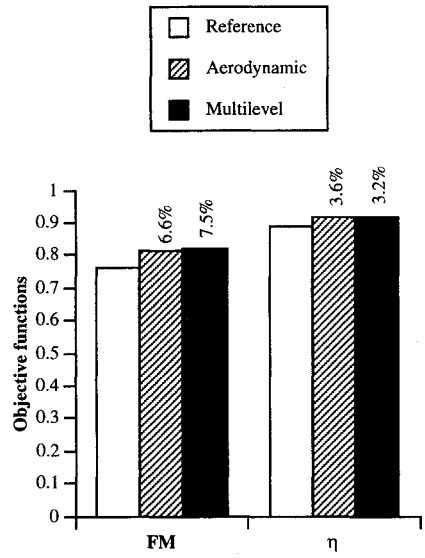

Fig. 4 Summary of upper level objective functions.

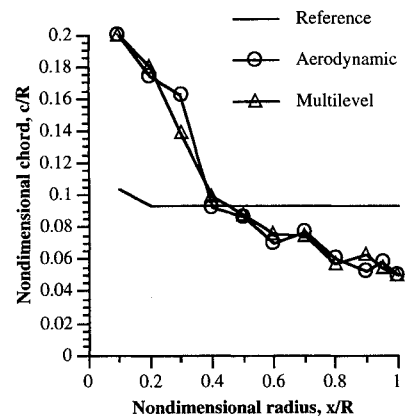

Fig. 5 Chord distributions.

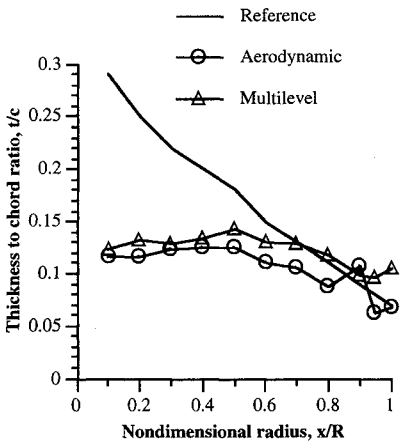

Fig. 6 Thickness to chord ratio distributions.

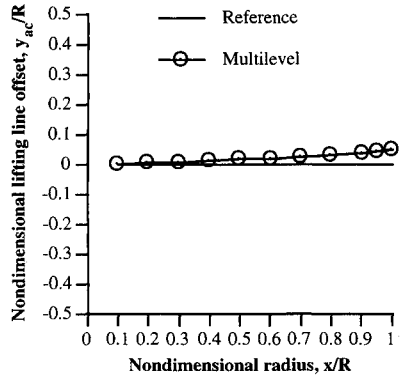

Fig. 7 Lifting line distributions.

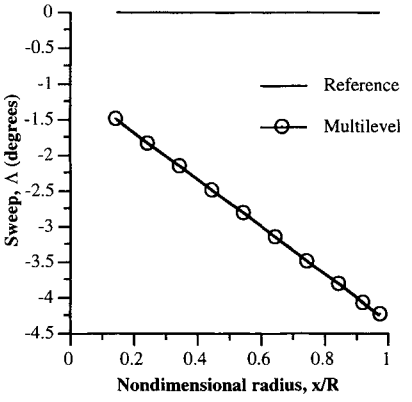

Fig. 8 Blade sweep distributions.

procedure the increase is slightly less (3.2%). These trends can be explained by examining the rotor planform.

The optimum and reference chord distributions c are shown in Fig. 5 where it is observed that the planforms obtained from both the aerodynamic and the multilevel optimization procedures are similar in shape and they differ sharply from the reference chord distribution. The optimum distributions closely resemble the well-known ideal hover planform. Such a distribution is the result of the large solidity requirement necessary to achieve the required thrust in hover. The reduction in the outboard section, relative to the reference rotor, is attributable to the lack of any maneuver margin requirement in the optimization problem formulation.

Figure 6 shows the t/c distributions for the three rotor configurations. From the figure, it is seen that there are large reductions from the reference rotor at the inboard sections in both of the optimum rotors. In case of the purely aerodynamic formulation, the optimum thickness is reduced from the reference blade throughout the blade span except at the 90% span location. This decrease represents an attempt to improve the rotor performance by reducing the profile drag. In case of the multilevel optimization procedure, similar trends are noted, only the reductions from the reference rotor are not as large. In fact, at the outboard section the airfoil thickness is actually increased from the reference values. The reason for these increases at the tip are to satisfy the constraint that ensures that the box beam can be contained within the airfoil. In case of the aerodynamic procedure, these constraints are violated at the tip. Since the multilevel procedure results in a thicker blade, compared to that from the aerodynamic optimization, the maximum coefficient of lift $C_{L\max}$ is increased in this design. This increase in $C_{L\max}$ subsequently improves the hover figure of merit, which explains the slight increase in FM from aerodynamic formulation. However, associated with the thicker airfoils are lower drag divergence Mach numbers M_{dd}, which cause the high-speed cruise performance to be slightly diminished, from the purely aerodynamic formulation.

The lifting line $y_{a/c}$ and sweep Λ distributions for the multilevel optimization and the reference rotor are presented in Figs. 7 and 8. Note that in the purely aerodynamic formulation, previously performed, no sweep modeling was included. As shown in Fig. 7, the lifting line is swept slightly forward, with the maximum offset at the tip. This results in the near-linear distribution of the sweep as shown in Fig. 7. This sweep distribution has the effect of increasing the torsional moment about the hub in an effort to reduce the elastic twist, which in this case is negative (nose down). It must be noted that forward sweep could adversely affect the aeroelastic stability and would have to be considered in a more comprehensive formulation including dynamic loads.

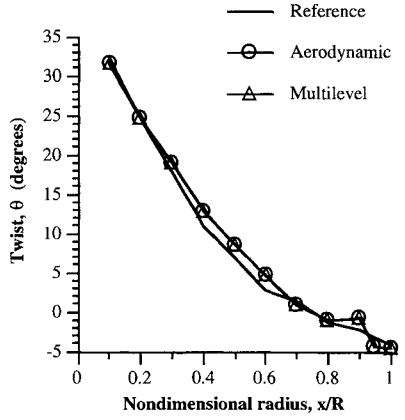

Fig. 9 Blade twist distributions.

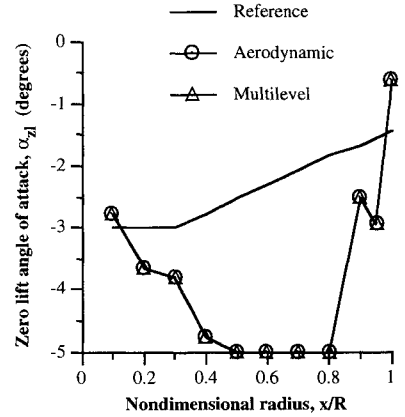

Fig. 10 Zero lift angle-of-attack distributions.

The θ and α_{z1} distributions are shown in Figs. 9 and 10. From the figure it is seen that the aerodynamic and the multilevel optimization results are nearly identical, varying only slightly from the reference distribution. The variations are most notable at the midspan locations where the optimum twist, through this region, is more linear than the reference rotor. This is due to the high-speed cruise requirements where more linear twist distributions are expected due to the high inflow velocity in forward flight. Figure 10 shows that the α_{z1} distributions for both the aerodynamic and the multilevel optimization procedures are nearly identical. However, in this case, both of these distributions vary drastically from the reference distribution. The figure shows that the optimum distributions are decreased significantly from the reference values at the inboard and midspan locations. This effectively increases the camber of the airfoil, which improves the airfoil lift-to-drag ratio, thereby improving performance. The zero lift angle of attack is then reduced (less camber) at the outboard section and is increased at the blade tip. This can be explained as the optimizer's attempt to avoid the reduction of M_{dd} to values below the operational Mach number at this location.

The nondimensional values of the lower level objective functions are presented in Fig. 11, where large deviations from the reference rotor are observed in the purely aerodynamic and multilevel optimization procedures. It should be noted here that the purely aerodynamic results were obtained without any structural considerations and the structural results presented here are computed using the results obtained from that study.[9] In the aerodynamic formulation it is seen that the elastic twist in hover ϕ_h, and in cruise ϕ_c, and the vertical displacement in hover w_h are significantly increased by 53, 61, and 6.5%, respectively, from the reference rotor. However, the horizontal displacement in cruise is actually decreased by 15%. In case of the multilevel optimization in which these displacements are included as objective functions, it is seen that there are significant reductions in all four displacements, from reference to optimum, after optimization. In this case, the elastic twist in hover and in cruise is reduced by 9.9 and 14%, respectively, and the vertical displacement in hover and the horizontal displacement in cruise are reduced by 16 and 3.9%, respectively. The magnitude of all the displacements are also reduced throughout the blade span from the reference values. An example of this is seen in Fig. 12, which displays the elastic twist deformations. This shows that in case of the multilevel formulation, even though the aerodynamic performance is comparable to the purely aerodynamic design (Fig. 4), the structural performance is greatly

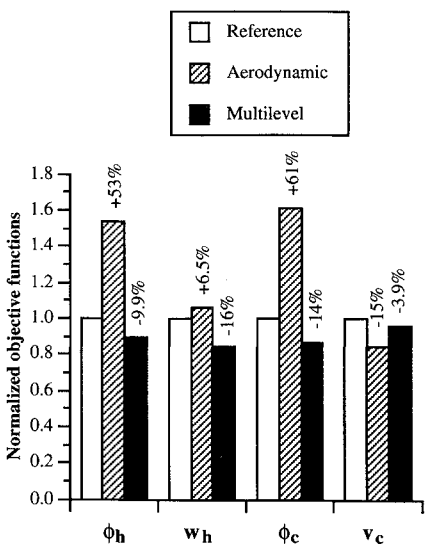

Fig. 11 Summary of lower level objective functions.

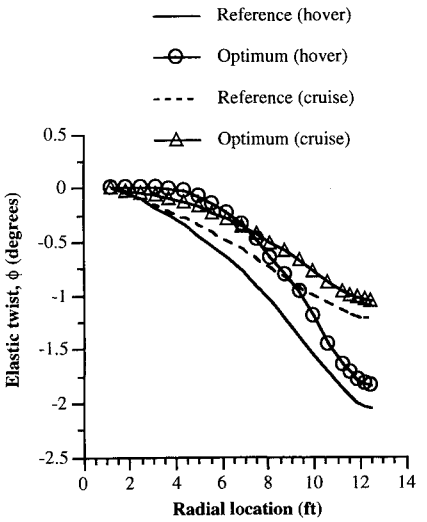

Fig. 12 Elastic twist distributions.

improved. These reductions are attributable to increased thickness of the airfoil, which in turn increases the height of the box beam, and also to the improved stacking sequence.

The composite laminate stacking sequences are presented in Table 1. Note that in the reference blade, the horizontal and vertical walls are assumed to have the same stacking sequence. Further, since all of the laminates are considered to be symmetric about their midplane, only 12 of the 24 total plies are presented in the table for each wall. The individual ply thickness used in this study is 0.01 in., which results in a total wall thickness of 0.24 in. For the sake of comparison, the structural response in case of the purely aerodynamic optimization formulation is obtained using the reference stacking sequence. Note that in the optimal configuration, there is a reduced number of ± 45-deg plies and an increased number of ± 30-deg plies. This can be explained as an attempt to compromise between the conflicting requirements of reduced elastic twist and reduced transverse displacements.

Concluding Remarks

A multilevel optimization procedure based on aerodynamic and structural performance is developed for an investigation of the coupled aerodynamic and structural design problem of high-speed prop-rotors. The classical blade element momentum approach is used for the aerodynamic analysis. The structural analysis is performed using a quasi-one-dimensional finite element approach based on a composite box beam model. At the upper level, a nonlinear programming technique based on the DFP method is used as the optimization algorithm. At the lower level, a discrete optimization based on the simulated annealing technique is used. The optimization problems are formulated using the K–S function approach. The optimum results obtained in this study are compared with a reference rotor and with a design obtained using a purely aerodynamic optimization procedure. Convergence is achieved after 147 total aerodynamic optimization cycles at the upper level and a total of 7000 simulated annealing iterations at the lower level. The following important observations are made.

1) The multilevel optimization procedure significantly improves aerodynamic and structural response of a high-speed prop-rotor blade. Further, the aerodynamic performance is comparable to a purely aerodynamic design demonstrating the success of the decomposition-based procedure.

2) The simulated annealing algorithm successfully minimizes the tip displacements by altering the composite plate stacking sequences in the horizontal and the vertical walls. The optimum composite stacking sequence represents a compromise between reduced elastic twist and reduced transverse

bending. This is manifested through the selection of ±30-deg plies in both the horizontal and vertical walls.

3) The airfoil t/c is increased from the purely aerodynamic formulation due to structural constraints on the blade. The thicker airfoil increases the hover performance with only a slight degradation in the cruise efficiency from the optimum aerodynamic results.

4) The optimum blade is swept slightly forward to improve the elastic twist. The sweep increases the torsional moment, which has the effect of reducing the nose down elastic twist.

5) The chord, twist, and zero lift angle of attack distributions differ significantly from the reference blade, but are very similar to the optimum aerodynamic configuration.

6) The elastic deformations at the blade tip as well as throughout the blade span are reduced from reference values. This is achieved through a combination of an improved ply-stacking sequence and slightly thicker airfoils.

Acknowledgments

This work was supported by NASA Ames Research Center, Moffett Field, California, Grant NCC2-795, Technical Monitor, John F. Madden III.

References

[1]Talbot, P., Phillips, J., and Totah, J., "Selected Design Issues of Some High Speed Rotorcraft Concepts," *AIAA/AHS/ASEE Aircraft Design, Systems and Operations Conference*, AIAA, Washington, DC, 1990, pp. 1167–1177 (AIAA Paper 90-3297).

[2]Rutherford, J., O'Rourke, M., Martin, C., Lovenguth, M., and Mitchell, C., "Technology Needs for High Speed Rotorcraft," NASA CR 177578, April 1991.

[3]Wilkerson, J. B., Schneider, J. J., and Bartie, K. M., "Technology Needs for High Speed Rotorcraft (1)," NASA CR 177585, May 1991.

[4]Chattopadhyay, A., and Narayan, J., "Optimum Design of High Speed Prop-Rotors Using a Multidisciplinary Approach," 48th Annual Forum of the American Helicopter Society, Washington, DC, June 1992.

[5]McCarthy, T. R., and Chattopadhyay, A., "Design of High Speed Proprotors Using Multiobjective Optimization Techniques," *Engineering Optimization*, Vol. 23, 1994, pp. 155–172; also AIAA Paper 93-1032, Feb. 1993.

[6]Chattopadhyay, A., McCarthy, T. R., and Madden, J. F., "Structural Optimization of High Speed Prop Rotors Including Aeroelastic Stability Constraints," *Mathematical and Computer Modelling, Special Issue on Rotorcraft*, Vol. 18, Nos. 3/4, 1993, pp. 101–113.

[7]Chattopadhyay, A., McCarthy, T. R., and Madden, J. F., "A Design Optimization Procedure for Minimizing Drive System Weight of High Speed Prop-Rotors," *Engineering Optimization*, Vol. 23, 1995, pp. 239–254.

[8]Chattopadhyay, A., McCarthy, T. R., and Madden, J. F., "An Optimization Procedure for the Design of Prop Rotors in High Speed Cruise Including the Coupling of Performance, Aeroelastic Stability and Structures," *Mathematical and Computer Modelling, Special Issue on Rotorcraft*, Vol. 19, Nos. 3/4, 1994, pp. 75–88.

[9]McCarthy, T. R., Chattopadhyay, A., Talbot, P. D., and Madden, J. F., "A Performance Based Optimization of High Speed Prop-Rotors," *Journal of the American Helicopter Society* (to be published); also *Proceedings of the American Helicopter Society Aeromechanics Specialists Conference* (San Francisco, CA), 1994.

[10]Kirkpatrick, S., Gelatt, C. D., Jr., and Vecchi, M. P., "Optimization by Simulated Annealing," *Science*, Vol. 220, No. 4598, 1983, pp. 671–680.

[11]Lamon, S., "XV-15 Advanced Technology Blades, Ultimate Stress Analysis," Boeing Rept. D210-12345-1, Philadelphia, PA, 1985.

[12]Talbot, P. D., "Propeller/Rotor Performance Code for Use in Preliminary Design," NASA Ames Research Center, ATTT Project Office Working Paper FPT WP 001, Moffett Field, CA, Nov. 1993.

[13]Smith, E. C., and Chopra, I., "Formulation and Evaluation of an Analytical Model for Composite Box-Beams," *Journal of the American Helicopter Society*, Vol. 36, No. 3, 1991, pp. 23–35.

[14]Walsh, J. L., Young, K. C., Pritchard, J. I., Adelman, H. M., and Mantay, W., "Multilevel Decomposition Approach to Integrated Aerodynamic/Dynamic/Structural Optimization of Helicopter Rotor Blades," *Proceedings of the American Helicopter Society Aeromechanics Specialists Conference* (San Francisco, CA), 1994, pp. 5.3-1–5.3-24.

[15]Chattopadhyay, A., McCarthy, T. R., and Pagaldipti, N., "Multilevel Decomposition Procedure for Efficient Design Optimization of Helicopter Rotor Blades," *AIAA Journal*, Vol. 33, No. 2, 1995, pp. 223–230.

[16]Kreisselmeier, A., and Steinhauser, R., "Systematic Control Design by Optimizing a Vector Performance Index," *Proceedings of the IFAC Symposium on Computer Aided Design of Control Systems* (Zurich, Switzerland), 1979, pp. 113–117.

[17]Tsai, S. W., and Wu, E. M., "A General Theory of Strength for Anisotropic Materials," *Journal of Composite Materials*, Vol. 5, No. 1, 1971, pp. 58–80.

[18]Smith, R. L., "Closed Form Equations for the Lift, Drag, and Pitching-Moment Coefficients of Airfoil Sections in Subsonic Flow," NASA TM 78492, Aug. 1978.

[19]Glauert, H., *The Elements of Aerofoil and Airscrew Theory*, 2nd ed., Cambridge Univ. Press, Cambridge, England, UK, 1948.

[20]Wrenn, G. A., "An Indirect Method for Numerical Optimization Using the Kreisselmeier–Steinhauser Function," NASA CR 4220, 1989.

[21]Olsen, G. R., and Vanderplaats, G. N., "Method for Nonlinear Optimization with Discrete Design Variables," *AIAA Journal*, Vol. 27, No. 1, 1989, pp. 1584–1589.

[22]Lombardi, M., Haftka, R. T., and Cinquini, C., "Optimization of Composite Plates for Buckling by Simulated Annealing," *Proceedings of the 33rd AIAA/ASME/ASCE/AHS/ASC Structures, Structural Dynamics, and Materials Conference* (Dallas, TX), AIAA, Washington, DC, 1992, pp. 2552–2562.

[23]Chattopadhyay, A., and Seeley, C. E., "A Simulated Annealing Technique for Multiobjective Optimization of Intelligent Structures," *Journal of Smart Material and Structures*, Vol. 3, Feb. 1994, pp. 98–106.

[24]Onoda, J., and Hanawa, Y., "Optimal Locations of Actuators for Statistical Static Shape Control of Large Space Structures: A Comparison of Approaches," *Proceedings of the AIAA/ASME/ASCE/AHS/ASC 33rd Structures, Structural Dynamics, and Materials Conference* (Dallas, TX), 1992, pp. 2788–2795.

[25]Agarwal, B. D., and Broutman, L. J., *Analysis and Performance of Fiber Composites*, Wiley, New York, 1990, p. 437.